Ferromagnetic and ferroelectric $5d^1$ insulator $Ba_5(OsO_5)_3Cl$

Cheng Tian (田程),[1,2] Dan Su (苏丹),[1,2] Shiyu Peng (彭士宇),[1,2] Jiashu Yan (闫家澍),[1,2] Thomas Doert,[3] Martin Jansen,[4] Zhijun Wang (王志俊),[1,2,*] Young Sun (孙阳),[1,5,†] Youguo Shi (石友国),[1,2,‡] and Hai L. Feng (冯海)[1,§]

[1]*Beijing National Laboratory for Condensed Matter Physics and Institute of Physics, Chinese Academy of Sciences, Beijing 100190, China*

[2]*School of Physical Sciences, University of Chinese Academy of Sciences, Beijing 100190, China*

[3]*Faculty of Chemistry and Food Chemistry, Technische Universität Dresden, Dresden, D-01069 Germany*

[4]*Max Planck Institute for Solid State Research, Stuttgart, D-70569 Germany*

[5]*Center of Quantum Materials and Devices, Chongqing University, Chongqing 401331, China*

(Received 4 June 2021; revised 6 October 2021; accepted 22 October 2021; published 10 November 2021)

Poly- and single-crystalline samples of $Ba_5(OsO_5)_3Cl$ have been successfully synthesized. $Ba_5(OsO_5)_3Cl$ crystallizes in the noncentrosymmetric space group $P6_3cm$. $Ba_5(OsO_5)_3Cl$ shows a ferromagnetic order below 5 K and a possible ferroelectric order below 150 K. A multiferroic state with both ferromagnetic and ferroelectric ordering is established, although the ferromagnetic and ferroelectric orders are not coupled. The experimental effective moment and the saturated magnetization for $Ba_5(OsO_5)_3Cl$ are close to the spin-only value, indicating that the spin-orbit coupling does not play an important role, which is due to the large crystal field and spin splitting in $Ba_5(OsO_5)_3Cl$.

DOI: 10.1103/PhysRevMaterials.5.114402

I. INTRODUCTION

Transition metal oxides (TMOs) with correlated electrons continue to attract great interest due to their fascinating magnetic and electrical properties. A general correlation for TMOs is that ferromagnetic (FM) TMOs are usually metallic and antiferromagnetic (AFM) TMOs are usually insulating. Among reported TMOs, the majority are AFM or ferrimagnetic, and FM TMOs are in the minority. FM TMOs, which are not metallic but insulating, are particularly rare [1].

Besides the FM insulator EuO [2], several FM insulators have been identified in the $3d$ double perovskite (DP) oxide family, such as La_2NiMnO_6 [3] and Bi_2NiMnO_6 [4], where FM orders are driven by the strong virtual hopping between empty and half-filled e_g orbitals according to the Goodenough-Kanamori rules [5]. In the search for FM insulators, DP Ba_2NiOsO_6 [6] and Ba_2NiIrO_6 [7] containing both $3d$ and $5d$ transition metal ions were synthesized and found to show a field-induced FM state. Calculations on Ba_2NiOsO_6 indicate that the spin-orbit coupling (SOC) plays an important role in the opening of the charge gap [6]. The compound $5d^1$ DP Ba_2NaOsO_6, reported to be FM insulator below 7 K, shows an anomalously small magnetization $\sim 0.2\,\mu_B$ at low temperatures and a negative Weiss temperature indicating dominant AFM magnetic interactions [8,9]. Recent studies indicate that Ba_2NaOsO_6 is a canted AFM [10]. For Ba_2NaOsO_6, the experimental effective moment (μ_{eff}) is in the range of 0.60–0.73 μ_B/Os^{7+}, so it is substantially reduced compared to the spin-only value of 1.73 μ_B expected for Os^{7+} ($5d^1$: $S = 1/2$).

In this work, we synthesized both poly- and single-crystalline samples of $Ba_5(OsO_5)_3Cl$ and found that $Ba_5(OsO_5)_3Cl$ is a $5d^1$ FM insulator below 5 K. We also demonstrate that $Ba_5(OsO_5)_3Cl$ displays a possible ferroelectric transition at 150 K. A multiferroic state with both ferromagnetic and ferroelectric ordering is established. The saturated magnetization for $Ba_5(OsO_5)_3Cl$ is close to the spin-only value of 1 μ_B/Os^{7+}. Theoretical calculations indicate that due to the large crystal field (CF) and spin splitting the SOC has little effect on the electronic band structure of $Ba_5(OsO_5)_3Cl$.

II. EXPERIMENT

Synthesis. Polycrystalline $Ba_5(OsO_5)_3Cl$ was synthesized by solid-state reactions. BaO, $BaCl_2$, and Os in the molar ratio of 4.5:0.5:3 were weighted and the mixture was thoroughly ground with a mortar and pestle. The starting mixture was loaded in a corundum crucible which was placed in a quartz tube. Another corundum crucible loaded with MnO_2 was placed in the same quartz tube. MnO_2 was served as an oxygen source, a MnO_2:Os molar ratio of 7:1 was applied. All these procedures were carried out in an Ar-filled glove box. The quartz tube was sealed under dynamic vacuum using a CO/O_2 torch, outside the glove box, and heated at 750 °C for 48 h. Single crystals of $Ba_5(OsO_5)_3Cl$ were grown from a flux. BaO and Os in a molar ratio of 5:3 (0.2 g in total) were well mixed with 4.5 g CsCl and KCl (CsCl:KCl weight ratio is 2:1) and loaded in a corundum crucible. Another corundum crucible loaded with MnO_2 was placed in the same quartz tube. MnO_2 served as an oxygen source; the MnO_2:Os molar ratio applied was 7:1. The quartz tube was sealed under

*wzj@iphy.ac.cn
†youngsun@cqu.edu.cn
‡ygshi@iphy.ac.cn
§hai.feng@iphy.ac.cn

a dynamic vacuum using a CO/O_2 torch, heated at 750 °C for 10 h, and then cooled slowly (2 °C/h) to 620 °C before turning off the furnace. The flux was removed by dissolving in distilled water.

X-ray diffraction. The polycrystalline $Ba_5(OsO_5)_3Cl$ sample was ground to a fine powder, which was then characterized by powder x-ray diffraction (PXRD) [Bruker D8 Advance (Cu $K\alpha$)]. Rietveld refinements of the powder diffraction data were carried out with the JANA2006 software [11]. Single-crystal x-ray diffraction (SCXRD) was performed with a four-circle diffractometer (Kappa Apex2, Bruker) equipped with a charge-coupled device (CCD) detector using graphite-monochromated Mo-$K\alpha$ radiation ($\lambda = 0.710\,73$ Å) at ambient temperature. Data were corrected for Lorentz and polarization factors [12] before applying a multiscan absorption correction [13]. The structure was solved with SUPERFLIP [14], implemented in the JANA2006 software. Structure refinement was performed with the program package JANA2006 against F2 including anisotropic displacement parameters for all atoms [11]. Crystal structures were drawn with the VESTA software [15].

Scanning electron microscopy (SEM) and energy-dispersive X-ray spectroscopy (EDX). SEM was performed with a SU8020 (Hitachi) with a triple-detector system for secondary electrons ($U_a = 2$ kV). The composition of selected single crystals was determined by semiquantitative energy dispersive x-ray analysis ($U_a = 20$ kV) with a silicon drift detector (SDD) $X - Max^N$ (Oxford). The stated composition reflects the average value of four EDX area measurements on a representative crystal.

Optical measurement. The optical measurement was performed at $T = 300$ K on a Bruker Vertex 80v spectrometer with photon energies up to 2500 meV. A single crystal of $Ba_5(OsO_5)_3Cl$ was cleaved to get a fresh surface. Its reflectance spectrum was measured using an *in situ* gold and aluminum overcoating technique.

Magnetism. The temperature dependence of the magnetic susceptibility was measured on a SQUID VSM-7T (Quantum Design Inc.). The measurements were conducted in field-cooling (FC) conditions with the temperature range of 2–300 K under an applied magnetic field of 1 T. Isothermal magnetization curves were measured at 2 K with fields between –7 and 7 T. The temperature dependence of specific heat was measured on a physical properties measurement system (PPMS-9T, Quantum Design Inc.) using the HC option with the relaxation method.

Dielectric, pyroelectric, and thermal expansion measurements. Dielectric permittivity and pyroelectric current were measured on polycrystalline samples in a cryogen-free superconducting magnet system (Oxford Instruments, TeslatronPT) using an LCR meter (Agilent 4980A) and an electrometer (Keithley 6517B), respectively. A poling procedure is necessary for the pyroelectric measurement. The sample was cooled down from 300 to 2 K under an electric field. After the electric field was removed and the samples were short circuited for 30 min, the pyroelectric current was measured with warming at a constant rate. The value of electric polarization was obtained by integrating the pyroelectric current with time. Thermal expansion was measured with a homemade capacitance dilatometer [16].

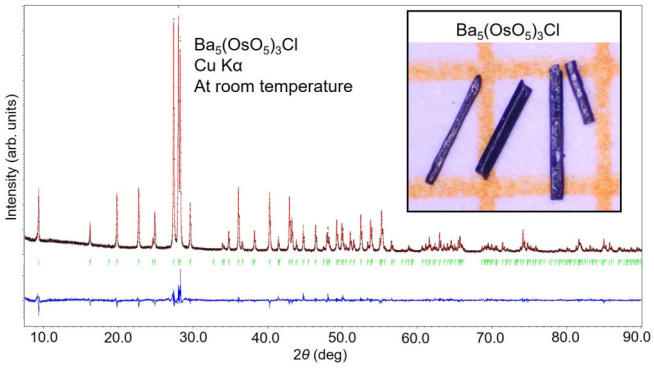

FIG. 1. PXRD patterns and Rietveld fitting of $Ba_5(OsO_5)_3Cl$. The inset shows a photograph of rodlike $Ba_5(OsO_5)_3Cl$ crystals on a millimeter grid.

Theoretical calculations. The first principle calculations based on density functional theory (DFT) have been performed through the Vienna ab *initio* simulation package (VASP) with the Perdew-Burke-Ernzerhof (PBE) generalized gradient approximation (GGA) exchange-correlation potential. A proper k mesh of $7 \times 7 \times 7$ is adopted and the energy cutoff of the plane wave is 550 eV. The Coulomb interaction is considered through the GGA+U method introduced by Dudarev *et al.* [17], and SOC is included within the second variational method for comparison.

III. RESULTS AND DISCUSSION

Crystal structures. Single- and poly-crystalline samples of $Ba_5(OsO_5)_3Cl$ were successfully synthesized. Rodlike single

TABLE I. Crystallographic data of $Ba_5(OsO_5)_3Cl$.

Empirical formula	$Ba_5(OsO_5)_3Cl$
Formula weight	1532.7 g/mol
Temperature	295(2) K
Radiation	Mo $K\alpha$ (0.71073 Å)
Crystal system	Hexagonal
Space group	$P6_3cm$ (No. 185)
Unit cell dimensions	$a = 10.9115(7)$ Å, $c = 7.8201(5)$ Å
Cell volume	806.33(9) Å^3
Z	2
Density, calculated	6.313 g/cm^3
$h\,k\,l$ range	$21 < h, k < 21, -15 < l < 15$
$2\theta_{min}/2\theta_{max}$	2.16/45.3
Linear absorption coefficient	35.771 mm^{-1}
Absorption correction	Multiscan
Number of reflections	68209
R_{int}	0.048
Number of independent reflections	2387
Number of observed reflections	2319 [$I > 3\sigma(I)$]
$F(000)$	1290
R values (all data)	R_1 : 1.65%
	wR_2 : 3.92
Weighting scheme	$w = 1/[\sigma^2(F_o^2) + 0.00576(F_o^2)]$
Flack parameter	0.001(5)
Min./max diff. Fourier	–0.81/1.57 e/Å^3
Refinement software	JANA2006

TABLE II. Atomic coordinates and equivalent displacement parameters for $Ba_5(OsO_5)_3Cl$.

Site	Wyckoff position	x	y	Z	U_{eq}(Å^2)
Os	6*c*	0.38944(1)	0	0.33510(4)	0.00695(3)
Ba1	4*b*	1/3	2/3	0.54927(4)	0.00762(4)
Ba2	6*c*	0.26188(2)	0	0.78308(3)	0.01022(5)
O1	6*c*	0.2946(4)	0	0.1576(5)	0.0210(10)
O2	12*d*	0.1304(2)	0.5775(2)	0.3030(3)	0.0135(5)
O3	12*d*	0.1321(2)	0.3881(2)	0.4810(3)	0.0121(5)
Cl	2*a*	0	0	0.0101(3)	0.0219(4)

crystals of $Ba_5(OsO_5)_3Cl$ were obtained (see the inset in Fig. 1). The structure of $Ba_5(OsO_5)_3Cl$ was first reported in 1995 [18]. Refinement of SCXRD data of $Ba_5(OsO_5)_3Cl$ as collected in this work converged well, confirming the hexagonal space group $P6_3cm$ as reported in the literature [18]. Refined cell parameters are $a = 10.9115(7)$ Å and $c = 7.8201(5)$ Å from single crystals and are in good agreement with the parameters reported [18]. Our structure determination confirms the literature data. Detailed crystal graphic data and atomic positions of single-crystal x-ray diffraction data are summarized in Tables I and II, respectively. Note that the atom coordinates have been transformed to the standard setting. The anisotropic displacement parameters are shown in the Supplemental Material [19]. The overall composition and the presence of Cl in the crystal structure are confirmed by EDX analysis on several $Ba_5(OsO_5)_3Cl$ crystals: Os 11.8(1) at. % (expected 12.5 at. %), Ba 19.2(3) at. % (20.8 at. %), Cl 3.4(1) at. % (4.17%), and O 65.6(4) at. % (62.5%). According to a Rietveld profile refinement of the PXRD pattern of polycrystalline $Ba_5(OsO_5)_3Cl$ (see Fig. 1), the powder samples are single phase and the refined cell parameters, $a = 10.9259(2)$ Å and $c = 7.8210(1)$ Å, are comparable to the ones obtained from single crystals.

The crystal structures of $Ba_5(OsO_5)_3Cl$ are shown in Fig. 2. Osmium is surrounded by five oxygen atoms, forming a slightly distorted tetragonal pyramid with four longer Os–O distances (about 1.838/1.844 Å) and one shorter distance [1.73 Å]. The OsO_5 pyramids are well separated from each other, such that no Os–O–Os superexchange path between them can be expected. The bond valence sum [20] calculated for Os is 7.07, supporting the nominal Os^{7+} oxidation state in $Ba_5(OsO_5)_3Cl$.

Direct band gap. The resistivity of $Ba_5(OsO_5)_3Cl$ is too large to measure by using the physical properties measurement system, indicating an insulating state. To estimate its band gap, we performed an infrared spectroscopy study on a $Ba_5(OsO_5)_3Cl$ single crystal at a temperature of 300 K. Figure 3 shows the real part of its optical conductivity spectrum σ_1 at 300 K, which was obtained by the Kramers-Kronig transformation of its reflectance spectrum [21]. As guided by the red dashed line in Fig. 3, the σ_1 increases sharply with the photon energy ω. The sharp increase above $\omega \sim 0.75$ eV in the $\sigma_1(\omega)$ can arise from the direct interband transition. The energy intercept of ~0.75 eV at $\sigma_1(\omega) = 0$ under a linear extrapolation of the $\sigma_1(\omega)$ represents a direct band gap of $Ba_5(OsO_5)_3Cl$ (see the red dashed line in Fig. 3) [21].

Magnetism. The temperature dependence of the FC magnetic susceptibility curves, $\chi(T)$, of $Ba_5(OsO_5)_3Cl$ single crystals [see Fig. 4(a)] shows sharp increases at low temperatures, indicating an FM-like transition. A T_c of ~5 K was determined from the minimum of the $d\chi/dT$ curves. $Ba_5(OsO_5)_3Cl$ shows a weak anisotropic behavior as the $\chi(T)$ curves measured with $H//c$ and $H\perp c$ deviate slightly at low temperatures. The $\chi(T)$ data in the range 10–300 K can be fitted with the modified Curie-Weiss law, $\chi = \chi_0 + C/(T-\theta_w)$ [see the inset of Fig. (4a)]. For the $H//c$ data $\chi_0 = -1.1 \times 10^{-3}$ emu/mol, $\mu_{eff} = 2.89\,\mu_B$/f.u., corresponding to $1.67\,\mu_B/Os^{7+}$, and θ_w of +4.0 K resulted. For the $H\perp c$ data $\chi_0 = -1.0 \times 10^{-3}$ emu/mol, $\mu_{eff} = 2.61\,\mu_B$/f.u., corresponding to $1.51\,\mu_B/Os^{7+}$, and a θ_w of +6.5 K was obtained. The weak anisotropic behavior is further confirmed by the

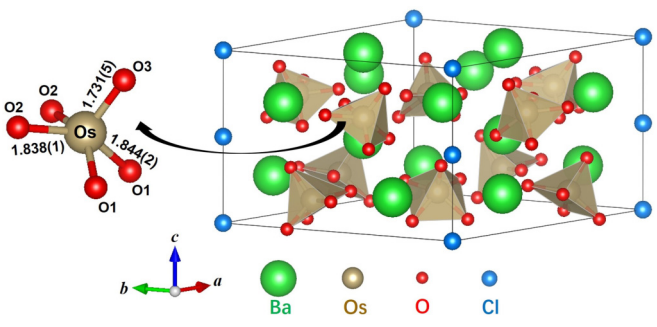

FIG. 2. Crystal structure of $Ba_5(OsO_5)_3Cl$.

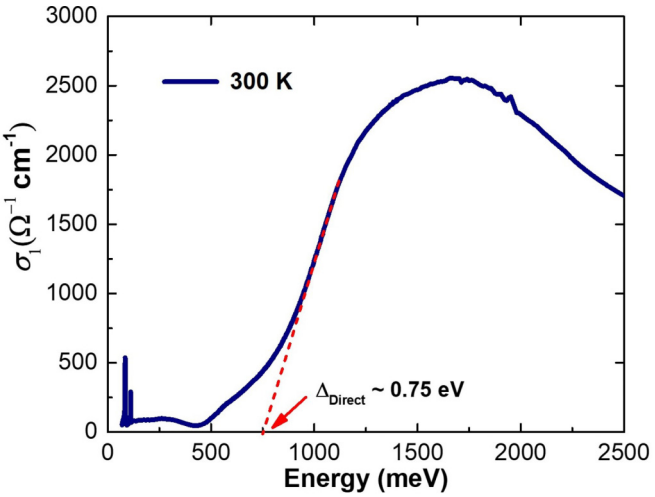

FIG. 3. Optical conductivity spectrum of the $Ba_5(OsO_5)_3Cl$ single crystal at 300 K.

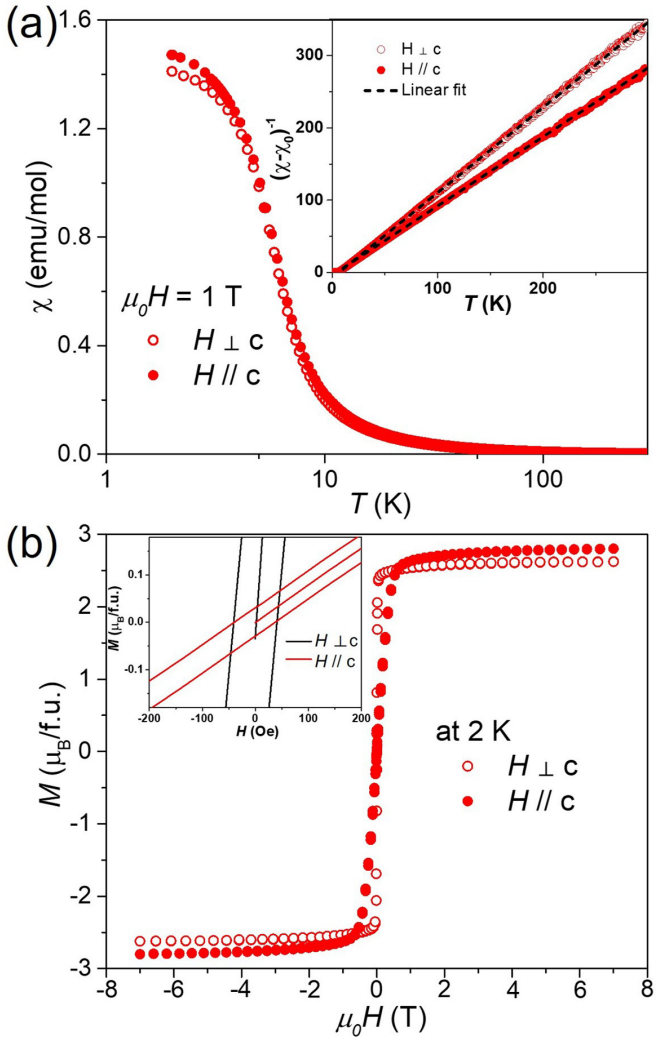

FIG. 4. (a) Temperature dependence of FC magnetic susceptibility curves, $\chi(T)$, of $Ba_5(OsO_5)_3Cl$ single crystals. Inset shows corresponding $(\chi - \chi_0)^{-1}$ vs T data. (b) Isothermal magnetization of $Ba_5(OsO_5)_3Cl$ single crystals at 2 K. Inset shows an enlarged view between –200 and 200 Oe.

isothermal magnetization curves of $Ba_5(OsO_5)_3Cl$ at 2 K as shown in Fig. 4(b). The magnetization is almost saturated with a value of 2.62 μ_B/f.u. when $H \perp c$, and with 2.80 μ_B/f.u. when $H//c$. The corresponding magnetizations are about 0.87 μ_B/Os^{7+} when $H \perp c$, and 0.93 μ_B/Os^{7+} when $H//c$, which are close to the spin-only value of 1 μ_B/Os^{7+} and support the FM order. It should be noted that $Ba_5(OsO_5)_3Cl$ is a very soft ferromagnet with a coercivity of about 40 Oe as shown in the inset of Fig. 4(b).

The temperature dependence of the FC magnetic susceptibility, $\chi(T)$, of polycrystalline $Ba_5(OsO_5)_3Cl$ is shown in Fig. S1(a) in the Supplemental Material [19]. In full correspondence with the single-crystal results, the polycrystalline sample displays an FM transition at ~5 K. The magnetization is almost saturated with a value of 2.68 μ_B/f.u., corresponding to 0.89 μ_B/Os^{7+} (see Fig. S1(b) in the Supplemental Material [19]). The 10–300 K $\chi(T)$ data can be fitted to a modified Curie-Weiss law, $\chi = \chi_0 + C/(T–\theta_w)$, where C is

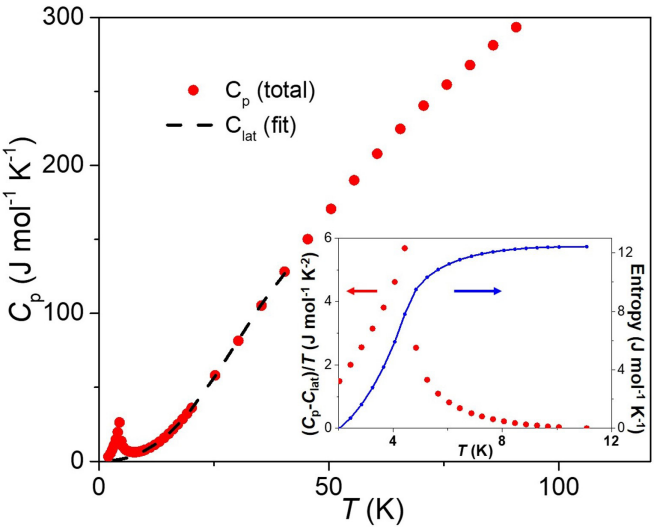

FIG. 5. Temperature-dependent specific heat of $Ba_5(OsO_5)_3Cl$. Inset shows the magnetic contribution and the corresponding entropy.

the Curie constant, θ_w is the Weiss temperature, and χ_0 is a temperature-independent term (see the inset of Fig. S1(a) in the Supplemental Material [19]). The fitting resulted in $\chi_0 = -4.5 \times 10^{-4}$ emu/mol, $\mu_{eff} = 2.67\ \mu_B$/f.u., corresponding to 1.54 μ_B/Os^{7+}, and an extracted θ_w of +8.0 K. The FM order was further confirmed to be of long-range nature as a sharp anomaly evolving around 5 K can be seen in the temperature-dependent specific heat curve (see Fig. 5). To estimate the magnetic entropy associated with the ferromagnetic transition, a polynomial fit to the data between 11 and 40 K was used to estimate the lattice contribution (C_{lat}) displayed as a dashed curve in Fig. 5. The corresponding temperature-dependent $(C_p - C_{lat})/T$ and entropy are shown in the inset of Fig. 5. The estimated magnetic entropy for $Ba_5(OsO_5)_3Cl$ is 12.4 J mol^{-1} K^{-1}, which is not far from the theoretical value

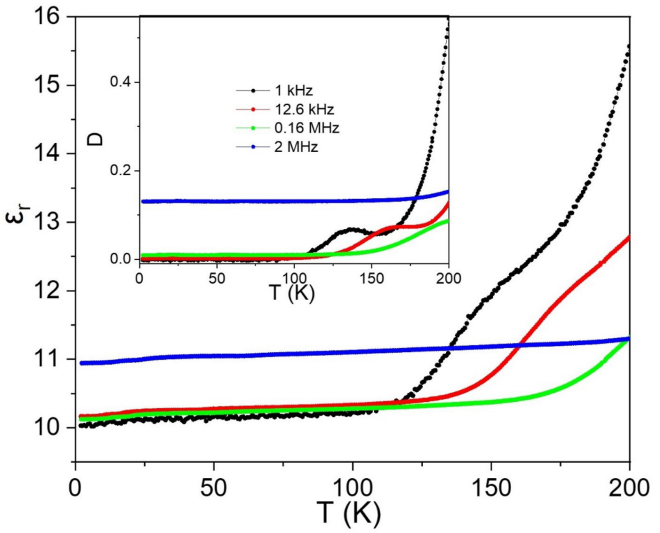

FIG. 6. The temperature dependence of the dielectric constant ε of $Ba_5(OsO_5)_3Cl$. The inset shows the temperature dependence of dielectric loss.

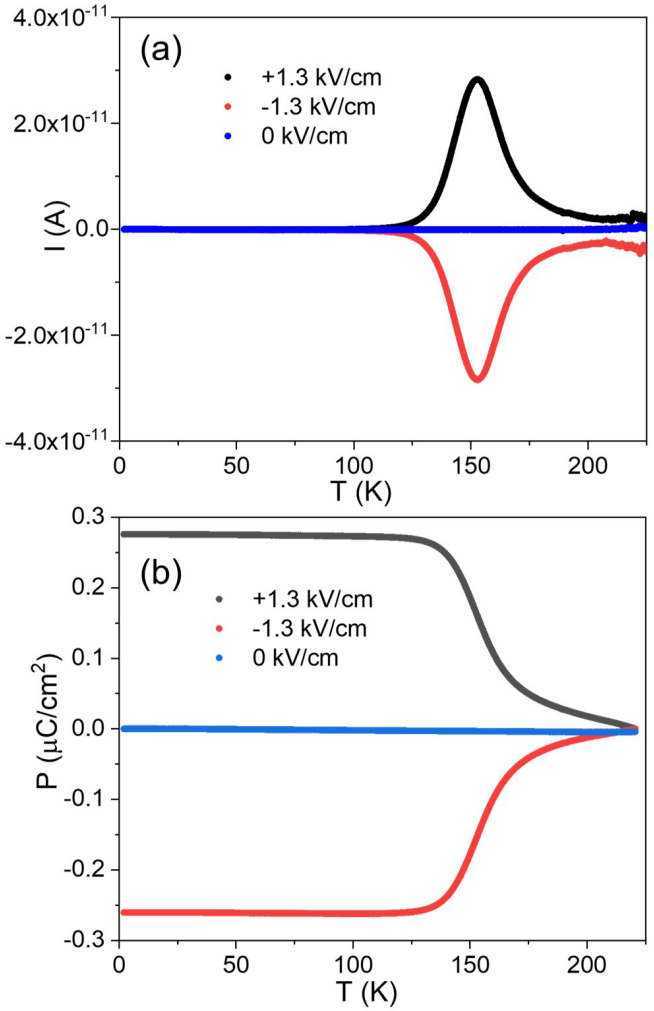

FIG. 7. (a) The temperature dependence of electric polarization of $Ba_5(OsO_5)_3Cl$ with different poling electric fields applied and (b) the corresponding pyroelectric data.

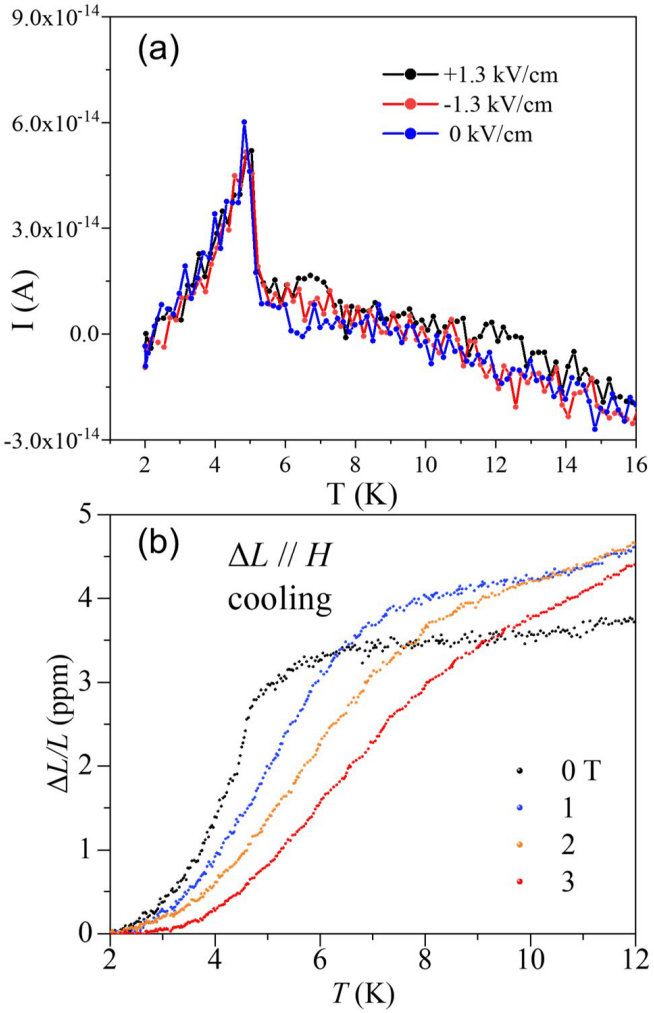

FIG. 8. (a) Low-temperature pyroelectric data. (b) Low-temperature thermal expansion measured under varied magnetic fields.

of 17.3 J mol^{-1} K^{-1} according to $3R\ln(2S+1)$, where R is the gas constant and $S = 1/2$ for Os^{7+}.

The obtained μ_{eff} of 1.54 μ_B/Os^{7+} (polycrystalline sample), 1.67 μ_B/Os^{7+} ($H//c$), and 1.51 μ_B/Os^{7+} ($H\perp c$) for $Ba_5(OsO_5)_3Cl$ are close to the spin-only value of 1.73 μ_B for an Os^{7+} ($5d^1$: $S = 1/2$). It should be noted that much-reduced μ_{eff} of 0.60–0.73 μ_B/Os^{7+} values have been reported for Ba_2NaOsO_6 and Ba_2LiOsO_6 due to strong SOC [8,9]. For $KOsO_4$ with $Os^{7+}O_4$ coordination, μ_{eff} of 1.4 μ_B/Os^{7+} was reported [22]. The difference may be due to the respective different local environments for osmium: $Os^{7+}O_5$ coordination for $Ba_5(OsO_5)_3Cl$, $Os^{7+}O_6$ coordination in Ba_2NaOsO_6 and Ba_2LiOsO_6, and $Os^{7+}O_4$ coordination in $KOsO_4$.

Positive θ_w values, +8.0 K for the polycrystalline sample, +4.0 K for $H//c$, and +6.5 K for $H\perp c$, indicate ferromagnetic interactions dominate in $Ba_5(OsO_5)_3Cl$, which is consistent with the FM ordering. These θ_w values are comparable with the T_c of 5 K, indicating the absence of magnetic frustration. The saturated magnetizations, 0.87–0.93 μ_B/Os^{7+}, are close to the spin-only ordered moment, 1.0 μ_B, for an Os^{7+} ($S = 1/2$), supporting the FM ordering.

Ferroelectricity. The temperature dependence of the dielectric constant, ε(T), measured at varied frequencies in zero magnetic fields, is shown in Fig. 6. ε(T) shows abnormal effects around 150 K, with the emerging humplike features in the corresponding dielectric loss (tanδ) curves (see the inset of Fig. 6). The dielectric anomalies shift to higher temperatures with increasing frequency. Considering the highly insulating nature and crystallographic group symmetry, the strong frequency-dependent characteristics in the dielectric properties may be indicative of a relaxor ferroelectric nature.

To further study the possible ferroelectric properties, temperature-dependent pyroelectric data measured at different poling electric fields are shown in Fig. 7(a). The sample is cooled in a 1.3 kV/cm E field from 300 to 2 K. After removing the electric field, the pyroelectric current is measured with warming at a rate of 5 K/min. A clear pyroelectric peak appears at approximately 150 K [see Fig. 7(a)], which is consistent with the dielectric anomaly. Integrating the pyroelectric current reveals a spontaneous electric polarization (P) to occur below 150 K with a value of about 0.27 $\mu C/cm^2$ [see Fig. 7(b)]. The observed polarization can be inverted with

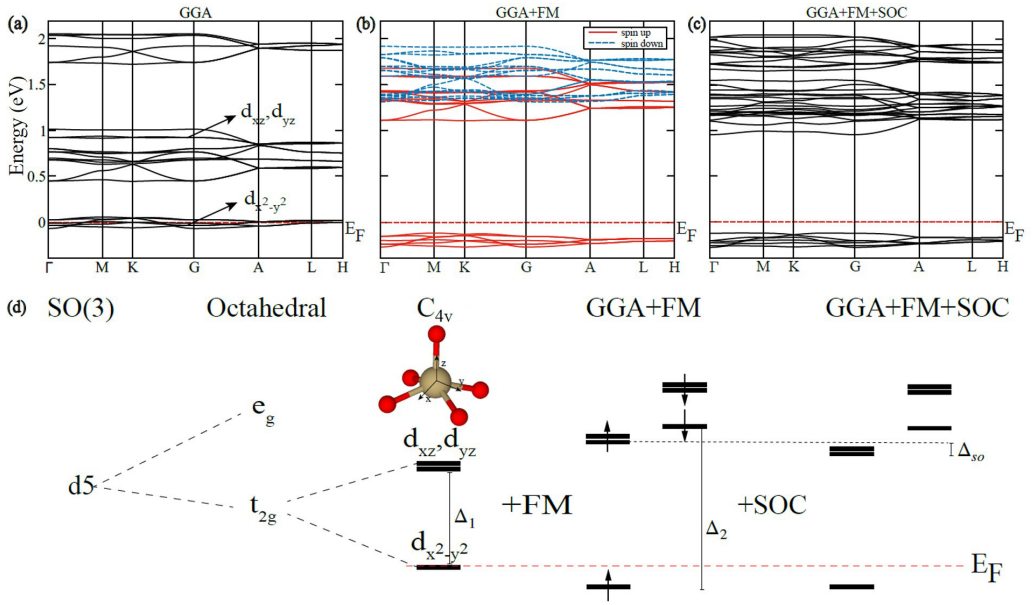

FIG. 9. Bulk band structure of GGA (a), GGA+FM ($U = 2.7$) (b), and GGA+FM+SOC (c). Spin-up and spin-down states are shown as red lines and blue dotted lines, respectively. (d) The schematic plot of splitting of five d orbitals in this compound. The adopted Cartesian coordinates of the pyramid are shown. Δ_1 is the energy splitting of the lower three orbitals under the C_{4v} symmetry of the pyramids (explicitly in its inset), Δ_2 is due to Zeeman coupling and Coulomb interaction U, and Δ_{so} is the energy change by spin-orbit coupling. E_F denotes the Fermi level.

opposite poling of the applied electric field, demonstrating the ferroelectric nature.

In addition to the broad pyroelectric signal around 150 K, another small peak evolves at 5 K, concomitant with the onset of FM order [Fig. 8(a)]. This peak does not change under different poling fields, indicating the presence of pyroelectricity rather than ferroelectricity. It seems that magnetic ordering induces a small change in electric polarization. The thermal expansion data demonstrate that there is a clear expansion of the lattice near the magnetic ordering temperature, as shown in Fig. 8(b). Therefore, the induced small electric polarization upon magnetic ordering is due to spin-lattice coupling. With increasing magnetic field, the rise in thermal expansion shifts to higher temperatures, further confirming the spin-lattice coupling in $Ba_5(OsO_5)_3Cl$.

DFT calculation. To begin with, the GGA band structure is shown in Fig. 9(a) with half-filled $d_{x^2-y^2}$ orbitals. It shows a large splitting ($\Delta_1 = 0.6$ eV) between $d_{x^2-y^2}$ and $d_{xz/yz}$ orbitals in the CF of the pyramids. Each Os atom in the crystal is surrounded by five O atoms, forming a pyramid with approximately C_{4v} point group symmetry. Octahedral CF split five d orbitals into e_g and t_{2g} orbitals, while C_{4v} symmetry will further split the lower three orbitals into a twofold set (d_{xz}, d_{yz}) and a single energy level ($d_{x^2-y^2}$). For FM state with Coulomb interaction ($U = 2.7$ eV), the Zeeman coupling will shift the spin-down states to a higher energy level (blue dashed lines) with respect to the spin-up states (red lines). $\Delta_2 = 1.48$ eV due to the Zeeman effect and Hubbard U interaction in Fig. 9(b). It gives rise to fully filled spin-up $d_{x^2-y^2}$ orbitals and empty spin-down $d_{x^2-y^2}$ orbitals, leading to an FM and insulating state. Besides, the GGA+FM+SOC band structure shows the SOC splitting of $\Delta_{so} = 0.1$ eV in Fig. 9(c). Due to the large CF and spin splitting, the SOC has little effect on its electronic band structures [see Fig. 9(d)]. Hence our *ab initio* calculations find that in $Ba_5(OsO_5)_3Cl$ the spin-up $d_{x^2-y^2}$ orbitals are occupied (no orbital moment) and the total magnetic moment should be fully contributed by the spin moment, resulting in a total magnetic moment of one μ_B ($\mu_{spin} = 0.977\,\mu_B$ and $\mu_{orb} = -0.042\,\mu_B$) for an Os^{7+} ion with $5d^1$ configuration, which agrees well with the experimental data.

IV. CONCLUSION

Poly- and single-crystalline samples of $Ba_5(OsO_5)_3Cl$ have been successfully synthesized. Both SCXRD and PXRD analysis confirm that $Ba_5(OsO_5)_3Cl$ crystallizes in the noncentrosymmetric space group $P6_3cm$. Magnetic and dielectric measurements indicate that $Ba_5(OsO_5)_3Cl$ shows an FM order below 5 K and a possible ferroelectric order below 150 K. A multiferroic state with both FM and ferroelectric ordering is established, although the FM and ferroelectric orders are not coupled. Magnetic measurements reveal that the experimental μ_{eff} and the saturated magnetization for $Ba_5(OsO_5)_3Cl$ are close to the spin-only value, indicating that SOC does not play an important role. The DFT calculations indicate that, due to the large CF and spin splitting, the SOC has little effect on electronic band structures of $Ba_5(OsO_5)_3Cl$.

ACKNOWLEDGMENTS

This study was supported by the Beijing Natural Science Foundation (No. Z180008 and No. Z180009), the National Natural Science Foundation of China (No. 12104492 and 11974395), the Strategic Priority Research Program of Chinese Academy of Sciences (Grant No. XDB33000000), and the Center for Materials Genome.

C.T., D.S., and S.P. contributed equally to this work.

[1] D. I. Khomskii and G. A. Sawatzky, Interplay between spin, charge and orbital degrees of freedom in magnetic oxides, Solid State Commun. **102**, 87 (1997).

[2] B. T. Mattias, R. M. Bozorth, and J. H. Van Vleck, Ferromagnetic Interaction in EuO, Phys. Rev. Lett. **7**, 160 (1961).

[3] N. S. Rogado, J. Li, A. W. Sleight, and M. A. Subramanian, Magnetocapacitance and magnetoresistance near room temperature in a ferromagnetic semiconductor: La_2NiMnO_6, Adv. Mater. **17**, 2225 (2005).

[4] M. Azuma, K. Takata, T. Saito, S. Ishiwata, Y. Shimakawa, and M. Takano, Designed ferromagnetic, ferroelectric Bi_2NiMnO_6, J. Am. Chem. Soc. **127**, 8889 (2005).

[5] J. B. Goodenough, *Magnetism and the Chemical Bond* (Interscience, New York, 1963).

[6] H. L. Feng, S. Calder, M. P. Ghimire, Y. H. Yuan, Y. Shirako, Y. Tsujimoto, Y. Matsushita, Z. W. Hu, C. Y. Kuo, L. H. Tjeng, T. W. Pi, Y. L. Soo, J. F. He, M. Tanaka, Y. Katsuya, M. Richter, and K. Yamaura, Ba_2NiOsO_6: A Dirac-Mott insulator with ferromagnetism near 100 K, Phys. Rev. B **94**, 235158 (2016).

[7] H. L. Feng, Z. Deng, C. U. Segre, M. Croft, S. H. Lapidus, C. E. Frank, Y. Shi, C. Jin, D. Walker, and M. Greenblatt, High-pressure synthesis of double perovskite Ba_2NiIrO_6: In search of a ferromagnetic insulator, Inorg. Chem. **60**, 1241 (2021).

[8] A. S. Erickson, S. Misra, G. J. Miller, R. R. Gupta, Z. Schlesinger, W. A. Harrison, J. M. Kim, and I. R. Fisher, Ferromagnetism in the Mott Insulator Ba_2NaOsO_6, Phys. Rev. Lett. **99**, 016404 (2007).

[9] K. E. Stitzer, M. D. Smith, and H. C. zur Loye, Crystal growth of Ba_2MOsO_6 (M = Li, Na) from reactive hydroxide fluxes, Solid State Sci. **4**, 311 (2002).

[10] L. Lu, M. Song, W. Liu, A. P. Reyes, P. Kuhns, H. O. Lee, I. R. Fisher, and V. F. Mitrovic, Magnetism and local symmetry breaking in a Mott insulator with strong spin orbit interactions, Nat. Commun. **8**, 14407 (2017).

[11] V. Petříček, M. Dušek, and L. Palatinus, Crystallographic computing system JANA2006: General features, Z. Kristallogr. – Cryst. Mater. **229**, 345 (2014).

[12] SAINT+: Area-detector integration software, v.8.38A (Bruker AXS Inc., Madison, WI, 2017).

[13] M. Sheldrick, *SADABS: Bruker/Siemens area detector absorption correction program, v.2016/2* (Bruker AXS Inc., Madison, WI, 2016).

[14] L. Palatinus and G. Chapuis, SUPERFLIP—a computer program for the solution of crystal structures by charge flipping in arbitrary dimensions, J. Appl. Crystallogr. **40**, 786 (2007).

[15] K. Momma and F. Izumi, VESTA 3 for three-dimensional visualization of crystal, volumetric and morphology data, J. Appl. Crystallogr. **44**, 1272 (2011).

[16] Y. Ma, Y. Wang, J. Cong, and Y. Sun, Magnetic-Field Tuning of Hydrogen Bond Order-Disorder Transition in Metal-Organic Frameworks, Phys. Rev. Lett. **122**, 255701 (2019).

[17] S. L. Dudarev, G. A. Botton, S. Y. Savrasov, C. J. Humphreys, and A. P. Sutton, Electron-energy-loss spectra and the structural stability of nickel oxide: An LSDA+U study, Phys. Rev. B **57**, 1505 (1998).

[18] J. R. Plaisier, R. A. G. Degraaff, and D. J. W. Ijdo, Structure determination of a new apatite—$Ba_5(OsO_5)_3Cl$, Mater. Res. Bull. **30**, 1249 (1995).

[19] See Supplemental Material at http://link.aps.org/supplemental/10.1103/PhysRevMaterials.5.114402 for anistropic displacement parameters for $Ba_5(OsO_5)_3Cl$ obtained from analysis of single-crystal x-ray diffraction data, and magnetic data for polycrystalline $Ba_5(OsO_5)_3Cl$.

[20] O. C. Gagné and F. C. Hawthorne, Comprehensive derivation of bond-valence parameters for ion pairs involving oxygen, Acta Crystallogr., Sect. B **71**, 562 (2015).

[21] Z. G. Chen, R. H. Yuan, T. Dong, G. Xu, Y. G. Shi, P. Zheng, J. L. Luo, J. G. Guo, X. L. Chen, and N. L. Wang, Inreared spectrum and its implications for the electronic structure of the semiconducting iron selenide $K_{0.38}Fe_{1.53}Se_2$, Phys. Rev. B **83**, 220507(R) (2011).

[22] S. Injac, A. K. L. Yuen, M. Avdeev, F. Orlandi, and B. J. Kennedy, Structural and magnetic studies of $KOsO_4$, a $5d^1$ quantum magnet oxide, Phys. Chem. Chem. Phys. **21**, 7261 (2019).